OXFORD

International Journal of Neuropsychopharmacology (2022) 25(10): 877–889

https://doi.org/10.1093/ijnp/pyac048
Advance Access Publication: July 30, 2022
Regular Research Article

REGULAR RESEARCH ARTICLE

Histone Deacetylase Inhibition Restores Behavioral and Synaptic Function in a Mouse Model of 16p11.2 Deletion

Wei Wang, MS, Tao Tan, PhD, Qing Cao, PhD, Freddy Zhang, BS, Benjamin Rein, PhD, Wei-Ming Duan, PhD, Zhen Yan, PhD

Department of Physiology and Biophysics, Jacobs School of Medicine and Biomedical Sciences, State University of New York at Buffalo, Buffalo, NY, USA (Ms Wang, Dr Tan, Dr Cao, Mr Zhang, Dr Rein, Dr Duan, Dr Yan).

Correspondence: Zhen Yan, PhD, University at Buffalo, JSMBS, 955 Main St., Buffalo, NY, 14203, USA (zhenyan@buffalo.edu).

Abstract

Background: Microdeletion of the human 16p11.2 gene locus confers risk for autism spectrum disorders and intellectual disability. How 16p11.2 deletion is linked to these neurodevelopmental disorders and whether there are treatment avenues for the manifested phenotypes remain to be elucidated. Emerging evidence suggests that epigenetic aberrations are strongly implicated in autism.
Methods: We performed behavioral and electrophysiological experiments to examine the therapeutic effects of epigenetic drugs in transgenic mice carrying 16p11.2 deletion (*16p11del*/+).
Results: We found that *16p11del*/+ mice exhibited a significantly reduced level of histone acetylation in the prefrontal cortex (PFC). A short (3-day) treatment with class I histone deacetylase (HDAC) inhibitor MS-275 or Romidepsin led to the prolonged (3–4 weeks) rescue of social and cognitive deficits in *16p11del*/+ mice. Concomitantly, MS-275 treatment reversed the hypoactivity of PFC pyramidal neurons and the hyperactivity of PFC fast-spiking interneurons. Moreover, the diminished N-methyl-D-aspartate (NMDA) receptor-mediated synaptic currents and the elevated $GABA_A$ receptor-mediated synaptic currents in PFC pyramidal neurons of *16p11del*/+ mice were restored to control levels by MS-275 treatment.
Conclusions: Our results suggest that HDAC inhibition provides a highly effective therapeutic strategy for behavioral deficits and excitation/inhibition imbalance in *16p11del*/+ mice, likely via normalization of synaptic function in the PFC.

Keywords: autism, behavior, 16p11.2 deletion, histone deacetylase, E/I balance

Introduction

Autism spectrum disorders (ASD), the prevalent neurodevelopmental diseases characterized by social, emotional, and communication deficits, have no effective treatment for the core symptoms. Human genetic screening has identified that many of the top-ranking autism risk factors are epigenetic enzymes regulating gene transcription through histone modifications and chromatin remodeling (De Rubeis et al., 2014; Satterstrom et al., 2020). Thus, we speculate that targeting epigenetic enzymes to normalize gene expression is a potential therapeutic strategy to mitigate behavioral defects in autism.

Microdeletion of the human 16p11.2 genetic locus (approximately 550 kb, approximately 27 genes) has been strongly linked

Received: March 15, 2022; **Revised:** June 21, 2022; **Accepted:** July 27, 2022

Significance Statement

Microdeletion of the human 16p11.2 gene locus confers risk for autism spectrum disorders and intellectual disability. This paper revealed that social and cognitive deficits in transgenic mice carrying 16p11.2 deletion (*16p11*$^{del/+}$) were ameliorated by a short treatment with class I histone deacetylase (HDAC) inhibitor MS-275 or Romidepsin. Concomitantly, the hypoactivity of pyramidal neurons and the hyperactivity of fast-spiking interneurons in prefrontal cortex (PFC) of *16p11*$^{del/+}$ mice were reversed by MS-275 treatment. Moreover, the diminished NMDA receptor-mediated synaptic currents and the elevated $GABA_A$ receptor-mediated synaptic currents in PFC pyramidal neurons of *16p11*$^{del/+}$ mice were normalized by MS-275 treatment. These results suggest that HDAC inhibition provides a highly effective therapeutic strategy for behavioral deficits in *16p11*$^{del/+}$ mice via the restoration of excitation/inhibition balance and synaptic function in the PFC.

to neurodevelopmental disorders, including ASD (Kumar et al., 2008; Weiss et al., 2008; Fernandez et al., 2010; Hanson et al., 2010; Rosenfeld et al., 2010; Shinawi et al., 2010; Zufferey et al., 2012). Transgenic mice carrying 16p11.2 deletions (*16p11*$^{del/+}$) display similar phenotypes to human patients with 16p11.2 deletions, including impairment in cognitive and memory tasks and deficits in social interaction and communication (Horev et al., 2011; Portmann et al., 2014; Yang et al., 2015a; Arbogast et al., 2016). Some of these behavioral abnormalities in 16p11.2 deletion mice are ameliorated by locus coeruleus activation (Yin et al., 2021), optogenetic activation of dorsal raphe 5-HT neurons, or activation of 5-HT1b receptors in the nucleus accumbens (Walsh et al., 2018). Emerging evidence indicates that aberrant synaptic functions in the prefrontal cortex (PFC), a brain region critical for high-level executive functions, is one of the pathophysiological mechanisms of ASD (Yan and Rein, 2022). Particularly, deficient NMDA receptor function and neuronal activity are found in PFC pyramidal neurons of *16p11*$^{del/+}$ mice, and chemogenetic stimulation of PFC activity ameliorates cognitive and social impairments in *16p11*$^{del/+}$ mice (Rein and Yan, 2020; Wang et al., 2018). Because disruption of excitation/inhibition (E/I) balance is a potential pathophysiological mechanism of autism (Sohal and Rubenstein, 2019), we speculate that other than changes in glutamatergic systems, the neuronal activity of GABAergic interneurons and GABAergic synaptic transmission in PFC is also altered in 16p11.2 deletion mice.

Transcriptomic studies have found that numerous genes are dysregulated by 16p11.2 deletion (Horev et al., 2011; Blumenthal et al., 2014; Ouellette et al., 2020), suggesting that molecular and cellular mechanisms underlying the autism-like behavioral deficits in 16p11$^{del/+}$ mice are complex. Given the critical role of histone modification in transcriptional regulation, we explored the epigenetic mechanism-based treatment strategy for 16p11.2 deletion syndrome. We focused on histone deacetylase (HDAC) family proteins, which generally silence gene expression via condensing the chromatin architecture. HDACs play a pivotal role in cognitive and emotional processes, and histone acetylation alteration and transcriptional dysfunction have been implicated in psychiatric disorders and autism (Tsankova et al., 2007; Contestabile and Sintoni, 2013; Yan and Rein, 2022). Our results demonstrate that administration of class I HDAC inhibitors leads to prolonged rescue of behavioral deficits in *16p11*$^{del/+}$ mice, which is accompanied by the restoration of E/I balance and synaptic function in the PFC.

MATERIALS AND METHODS

Animals and Reagents

All animal experiments were performed with the approval of the Institutional Animal Care and Use Committee of the State University of New York at Buffalo. The 16p11.2 deletion mice (*16p11.2*$^{del/+}$) were generated as we previously described (Wang et al., 2018). In brief, 16p11.2 deletion mice (16p11.2$^{del/+}$) were generated with the deletion of 1 copy (heterozygous for a deletion or deficiency allele) of the syntenic 440-kbp region on mouse chromosome 7F3 corresponding to human chromosome 16p11.2 region (Horev et al., 2011). Heterozygous 16p11.2$^{del/+}$ female mice (The Jackson Laboratory, Stock # 0251000) were bred with wild-type (WT; C57BL/6N129Sv, The Jackson Laboratory, Stock #101043) male mice to generate heterozygous offspring for experimental use. Mice were maintained in the animal facility under controlled environmental conditions (22°C, 12-hour-light/-dark cycle) with free access to food and water. Both male and female mice (6–10 weeks old) of 16p11$^{del/+}$ and WT were randomly assigned to different groups.

Experiments were carried out by researchers in a blind manner (with no prior knowledge about the groups and treatments). Different groups were coded with A, B, C, and D. The operator who conducted the behavioral test was given only the coded group. After analyzing the behavioral data, it was decoded into the assigned groups.

MS-275 (Selleckchem) and romidepsin (Selleckchem) were prepared by dissolving into DMSO to make stock solutions and diluting with 0.9% saline before injections (final DMSO concentration of the working solution: <0.2%). MS-275 (5 mg/kg) or Romidepsin (1 mg/kg) was systemically (i.p.) administered once daily for 3 consecutive days.

Immunohistochemistry

Mice were deeply anesthetized and transcardially perfused with PBS followed by 4% paraformaldehyde (pH = 7.4). Brains were post-fixed in 4% PFA at 4°C for 24 hours and then transferred to 30% sucrose solution. After immersion in sucrose for 3 days, brains were coronally cut into 40-μm slices with a vibratome (Leica VP1000S, Leica Microsystems Inc., Wetzlar, Germany). Slices containing PFC were washed and blocked for 1 hour in PBS containing 5% BSA and 0.3% Triton. After washing, slices were incubated with the primary antibody against H3K9Ac (1:500, 9649S, Cell Signaling Technology) or NeuN (1:500, MAB377, Millipore Burlington, MA) for 12–15 hours at 4°C. After washing 3 times in PBS, slices were incubated with the secondary antibody (Alexa Fluor 488, 1:1000, A11008, Invitrogen, Waltham, MA) or (Alexa Fluor 594, 1:1000, A11032, Invitrogen) for 1 hour at room temperature, followed by 3 washes with PBS. Slices were mounted on slides with VECTASHIELD mounting medium (Vector Laboratories). Images were acquired using a 63× objective lens on a confocal microscope (Leica TCS SP8). All specimens were imaged under identical conditions and analyzed with identical parameters using Image J (NIH). For measuring the H3K9Ac level, a threshold was used to remove the background signal on the Z-axis projected image and the H3K9Ac fluorescence intensity of the whole image was detected.

Western Blotting

Nuclear extracts from mouse brains were prepared as we previously described (Qin et al., 2018; Zhang et al., 2021). Briefly, PFC punches from mouse slices were collected, then homogenized with 500 µL hypotonic buffer (20 mM Tris-HCl, pH 7.4, 10 mM NaCl, 3 mM $MgCl_2$, 0.5% nonyl phenoxypolyethoxylethanol [NP-40, tergitol-type], 1 mM phenylmethylsulfonyl fluoride [PMSF], with cocktail protease inhibitor). The homogenate was incubated on ice for 15 minutes and then centrifuged at 3000 g for 10 minutes at 4°C. The nuclear pellet was resuspended in 50 µL nuclear extract buffer (100 mM Tris-HCl, pH 7.4, 100 mM NaCl, 1 mM EDTA, 1% Triton X-100, 0.1% SDS, 10% glycerol, 1 mM PMSF, with cocktail protease inhibitor) and incubated on ice for 30 minutes with periodic vortexing to resuspend the pellet. After centrifugation, the supernatant for nuclear fractions was collected, boiled in 2 × SDS loading buffer for 5 minutes, separated on SDS-polyacrylamide gels, and then transferred to nitrocellulose membranes with the Fast-transfer system (Bio-Rad). Membranes were incubated with the primary antibody against pan-acetylated H3 (1:1000, 9441S, Cell Signaling Technology) or H3 (1:1000, 4499S, Cell Signaling Technology) at 4°C overnight. After washing, membranes were incubated with a horseradish peroxidase-conjugated anti-rabbit IgG secondary antibody (1:2000, NA934, GE Lifesciences) for 1 hour at room temperature. Blots were developed using enhanced chemiluminescence substrate (SuperSignal West-Pico, Thermo Fisher). Images and data were acquired with Chemidoc XRS system (Bio-Rad). Analysis was performed using ImageJ software (NIH). H3 was used as the loading control, and the amount of H3Ac expression was normalized to the amount of total H3.

Behavioral Tests

The room light was adjusted to dim during all behavioral experiments except for Barnes maze tests. ANY-maze 5.1 (Stoelting) was used for animal tracking and data analysis. Operators were blind to experimental groups during testing and scoring. Animals were habituated to the experimental room in their home cages for at least 30 minutes before testing. Mice were returned to the home cages between trials to rest. To mask olfactory cues, all testing apparatuses were cleaned with 75% ethanol.

***Social Approach Test*—**The test animal was habituated in an apparatus (length, 67.7 cm; width, 50.8 cm; height, 50.8 cm) containing a capsule (an inverted pencil cup) for 10 minutes and then was returned to the home cage (Qin et al., 2018; Wang et al., 2018). After cleaning the apparatus, a social stimulus (an age- and sex-matched wild-type counterpart) was placed into the capsule. The test animal was then returned to the apparatus for a 10-minute free exploration. The time spent interacting with the social stimulus and the number of approaching the social stimulus were measured.

***Lomotion Test*—**The animal was placed in a transparent plastic cage (40 × 40 × 30 cm) equipped with an infrared motion-sensor system (AccuScan Instruments Inc.). Locomotor activity was monitored by using VersaMax animal activity software (Omnitech Electronics, Inc.). Total distance traveled and time spent in center during a 30-minute test were recorded and analyzed. The corn cob bedding in the cages was cleaned after each test session.

***Barnes Maze Test*—**The test animal was placed on a round platform (36-inch diameter) with 8 equally spaced holes at the edge, one of which was attached with an escape box (Cao et al., 2020). A weak aversive light stimulation was applied to increase the motivation to escape from the circular platform and enter the escape box. During the learning phases, the animal was allowed to explore the platform until it found the correct hole and entered the escape box using distal visual cues. The interval between each learning phase was 5 minutes. After 2 learning sessions, the animal was placed back in its home cage for 15 minutes. In the memory test phase, the escape box was removed, and the animal was placed on the platform for a 3-minute exploration. The amount of time spent around the correct hole (T1) and incorrect holes (T2, the other 7 holes) were measured. The spatial memory index was calculated by T1/T2.

***Novel Object Recognition Test*—**After habituation on a round platform (24-inch diameter) for 5 minutes, the mouse was allowed to explore 2 identical objects on the platform for 5 minutes. After a 5-minute break in the home cage, the mouse was brought back to explore the platform with an original familiar object and a novel object for 5 minutes. The time spent with each object was counted. The discrimination ratio was calculated by $(T_N - T_F)/(T_N + T_F)$, where T_N and T_F indicate the time spent with the novel and familiar object, respectively. All the objects used in each repeated measurement at different time points were unique without repeat.

Electrophysiological Recording

***In Vivo Recording in Anesthetized Mice*—**Multichannel recording of in vivo spike activity used a similar approach as previously described (Tan et al., 2021). Mice were anesthetized with ketamine (100 mg/kg)/xylazine (10 mg/kg, i.p.). Animal body temperature was maintained at 36.5°C ± 1°C. After a craniotomy (1- × 2-mm rectangle) was made directly above the medial PFC (+1.98 mm AP, ±0.25 mm ML, –2.2 mm DV), the dura was removed. A multichannel recording probe (NeuroNexus, A1x16-5mm-50-177-A16, 16 channels) was inserted radially via a small durotomy. By positioning the electrode tip 2.2–2.5 mm deep from the brain surface, the probe was advanced into the target brain region and allowed to settle until the stable activity was observed for 10–15 minutes, and the units were recorded. Recordings were amplified and digitized at 30 kHz (Intan 512ch Recording Controller with RHD2132 16-channel headstage). Spikes were separated with a band-pass filter at 250–7500 Hz. Spikes were detected using an amplitude threshold (2.8-5 standard deviation [SD] of background activity). Spike clustering was performed with Plexon Offline Sorter (Plexon) and further analyzed with MATLAB (MathWorks). Units with a low signal-to-noise (<3.0) were discarded.

***Whole-Cell Recording in Brain Slices*—**Whole-cell voltage-clamp and current-clamp recordings were used to measure synaptic currents and action potentials in medial PFC layer V pyramidal neurons and layer II and III interneurons, as we previously described (Zhong and Yan, 2016; Qin et al., 2018; Wang et al., 2018). Mouse brain slices (300 µm) were positioned in a perfusion chamber attached to the fixed stage of an upright microscope (Olympus) and submerged in continuously flowing oxygenated (95% O_2 and 5% CO_2) ACSF (in mM: 130 NaCl, 26 $NaHCO_3$, 1 $CaCl_2$, 5 $MgCl_2$, 3 KCl, 1.25 NaH_2PO_4, 10 glucose, pH 7.4, 300 mOsm). Cells were visualized with a water-immersion lens (40×) and a CCD camera. A Multiclamp 700 A amplifier with Clampex 8.2 software and Digidata1322A (Molecular Devices) was used for recordings. Recording pipettes were pulled from glass capillaries (1.5 mm OD and 0.86 mm ID) with resistance at 3–5 MΩ by a pipette puller (Model P-97, Sutter Instrument Co.).

For NMDAR-mediated EPSC recordings, the internal solution contained (in mM: 130 Cs-methanesulfonate, 10 CsCl, 4 NaCl, 10 HEPES, 1 $MgCl_2$, 5 EGTA, 2 QX-314, 12 phosphocreatine, 5 MgATP,

0.2 Na_3GTP, 0.1 leupeptin, pH 7.2-7.3, 265-270 mOsm). Bicuculline (20 μM) and CNQX (25 μM) were added to ACSF. Neurons were depolarized to +40 mV for 3 seconds before stimulation to remove Mg^{2+} block. For $GABA_AR$-mediated IPSC recordings, the internal solution contained (in mM) 100 CsCl, 30 N-methyl-D-glucamine, 10 HEPES, 4 NaCl, 1 $MgCl_2$, 5 EGTA, 2 QX-314, 12 phosphocreatine, 5 MgATP, 0.5 Na_2GTP, pH 7.2–7.3, 265–270 mOsm. D-APV (25 μM) and CNQX (25 μM) were added to ACSF. Neurons were held at –70 mV. For mIPSCs recording, TTX (1 μM) was added to the external solution. Evoked EPSC or IPSC was elicited by a series of current pulses with different stimulation intensities (20–110 μA, delivered at 0.05 Hz) from an S48 stimulator (Grass Technologies) via a bipolar stimulating electrode (FHC) placed at approximately 100 μm from the recorded neuron. Paired-pulse ratio (PPR) was evoked by 2 pulses with different intervals (30–300 ms).

For spontaneous action potential recordings, slices were bathed in a modified ACSF (0.5 mM $MgCl_2$, 3.5 mM KCl) to slightly elevate the basal neuronal activity. The internal solution contained (in mM: 20 KCl, 100 K-gluconate, 10 HEPES, 4 ATP, 0.5 GTP, and 10 phosphocreatine). A small depolarizing current was applied to adjust the inter-spike potential at approximately –58 mV (Zhong and Yan, 2016). For evoked action potential recording, membrane potential was held to –70 mV with the injection of a series of depolarizing currents (0–300 pA).

Electrophysiological data were analyzed with Clampfit 10.0.7 (Molecular Devices) and Mini Analysis 6.0.3 (Synaptosoft).

Quantitative Real-Time PCR

To compare mRNA levels, real-time quantitative (qPCR) was used (Qin et al., 2018). Total RNA was isolated from mouse PFC punches using Trizol reagent (Invitrogen) and treated with DNase I (Invitrogen) to remove genomic DNA. Then iScriptTM cDNA synthesis Kit (Bio-Rad) was used to obtain cDNA from the tissue mRNA. qPCR was carried out using iCycler iQ RealTime PCR Detection System and iQ Supermix (Bio-Rad) according to the manufacturer's instructions. GAPDH was used as the housekeeping gene for quantification of the expression of target genes. Fold changes in the target genes were determined by: fold change = $2^{-\Delta(\Delta Ct)}$, where $\Delta Ct = Ct(target) - Ct(GAPDH)$, and $\Delta(\Delta Ct) = \Delta Ct(16p11^{del/+}) - \Delta Ct(WT)$. Ct (threshold cycle) is defined as the fractional cycle number at which the fluorescence reaches 10× the SD of the baseline. A total reaction mixture of 20 μL was amplified in a 96-well thin-wall PCR plate (Bio-Rad) using the following PCR cycling parameters: 95°C for 5 minutes followed by 40 cycles of 95°C for 45 seconds, 55°C for 45 seconds, and 72°C for 45 seconds. Primers for all target genes are listed here.

Gene	Species	Forward Primer	Reverse Primer	Accession No.
Mapk3	Mouse	TATCAACACCACCTGCGACC	GGATTTGGTGTAGCCCTTGGA	NM_011952.2
Slc6a1	Mouse	GGCCGCAGGCTCTGT	GTGGGCGCGAGATGTCAG	NM_178703.4
Vgat	Mouse	GCCATTCAGGGCATGTTCG	TGAGGATCTTGCCGGTGTAG	NM_009508.2
Gad65	Mouse	CGTGTATGGGGCTTTTGATCC	TCAGTCCCTCCTCTCTAACCAG	NM_008078.2
Gabra1	Mouse	CACCATGAGGTTGACCGTGA	CTACAACCACTGAACGGGCT	NM_010250.5
Gabrb2	Mouse	ATTTGGTGGCTCAAACGGTC	GAGATTTCCTCACCAGCAGGA	NM_008070.4
Gabrg2	Mouse	GGAGCCGGCATCAAATCATC	CTTTTGGCTTGTGAAGCCTGG	NM_008073.4
Npas4	Mouse	ACCTAGCCCTACTGGACGTT	CTTTCAGCCAACAGGCGGTA	NM_153553.5
Pvalb	Mouse	GCTTTTCTGTATAGGCTCCGGC	TCAGAATGGACCCCAGCTCATC	NM_013645.4
Arc	Mouse	GAGGCTCAGCAATATCAGTC	GGACAGCCAATATTCTTCAG	NM_018790.3
Gapdh	Human	AGATCCCTCCAAAATCAAGT	CAGAGATGATGACCCTTTTG	NM_002046

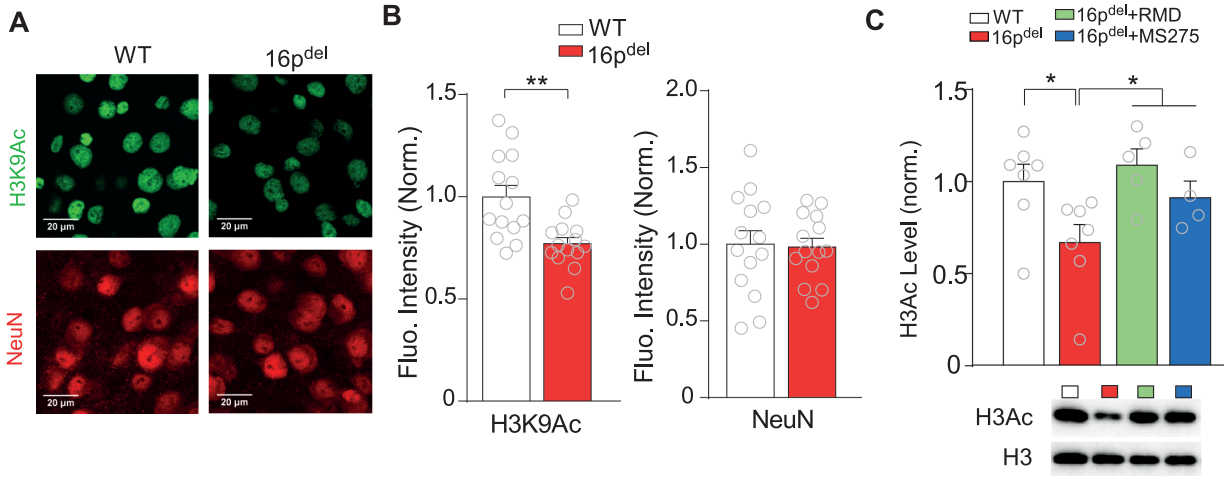

Figure 1. *16p11.2del/+* mice exhibited the reduced histone acetylation in PFC, which was restored by treatment with class I HDAC inhibitors. (A) Confocal images (120×) of H3K9Ac (green) and NeuN (red) staining in PFC slices from wild-type (WT) and *16p11.2del/+* (16p^{del}) mice. (B) Quantification of the integrated intensity of H3K9Ac and NeuN signals in WT and *16p11.2del/+* mice (n = 14 slices/5 mice/group, $t_{(26)} = 3.6$, $P = .0013$, unpaired *t* test). (C) Quantification and representative western-blot images of acetylated H3 in the nuclear fraction of PFC slices from WT or *16p11.2del/+* mice without or with the treatment of romidepsin (RMD, 1 mg/kg, i.p., 3×) or MS-275 (5 mg/kg, i.p., 3×) (n = 4–7 samples/group, $F_{2,20} = 5.0$, $P = .02$, 1-way ANOVA). All data are presented as mean ±SEM. In all figures, *$P < .05$, **$P < .01$.

Statistics

GraphPad Prism 8.0.1 (GraphPad Software) was used for the statistical analysis of the data. All data were presented as means ± SEM. Experiments with 2 groups were analyzed using *t* tests (2-tailed, unpaired or paired). Experiments with more than 2 groups were subjected to 1-way or 2-way ANOVA or 1-way or 2-way repeated-measure ANOVA followed by Bonferroni post hoc tests for multiple comparisons. All data are presented as mean ± SEM.

RESULTS

Histone Acetylation Is Reduced in PFC of *16p11.2del/+* Mice

Histone hypoacetylation has been found in the PFC of Shank3-deficient mouse models of autism and postmortem autistic patients (Qin et al., 2018, 2021a). To determine whether histone acetylation is also changed in *16p11.2*$^{del/+}$ mice, we performed immunostaining of acetylated histone 3 in PFC slices. As shown

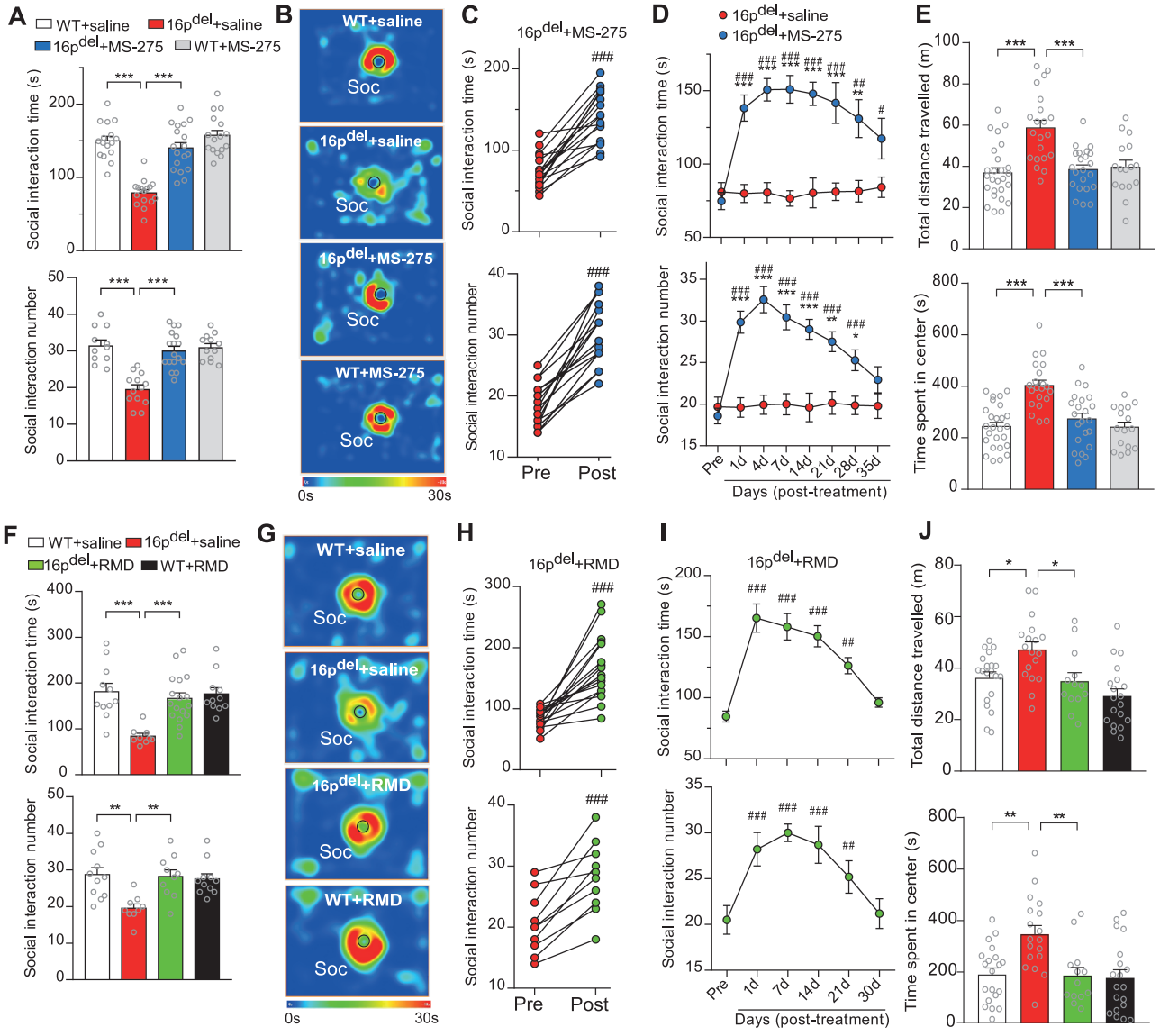

Figure 2. Treatment with HDAC inhibitors induces prolonged rescue of social deficits and mitigates hyperlocomotion in *16p11.2del/+* mice. (A, F) Bar graphs of social interaction time and number during social approach tests of WT vs *16p11.2del/+* mice treated with saline or MS-275 (5 mg/kg, i.p., 3×) or romidepsin (RMD) (1 mg/kg, i.p. 3×) (A, time: n = 16–18 mice/group, $F_{1,62(interaction)} = 18.0$, $P < .0001$; number: n = 11–17 mice/group, $F_{1,49(interaction)} = 19.7$, $P < .0001$; F, time: n = 9–17 mice/group, $F_{1,37(interaction)} = 9.4$, $P = .0036$; number: n = 9–11 mice/group, $F_{1,37(interaction)} = 8.8$, $P = .0053$, 2-way ANOVA). (B, G) Representative heatmaps illustrating the topographical time distribution in social approach tests of different groups. (C, H) Scatter plots of social interaction time and number of individual *16p11.2del/+* mice before and after MS-275 or RMD treatment (C, n = 17 mice, time: $t_{(16)} = 8.7$, $P < .0001$; number: $t_{(16)} = 10.5$, $P = .0003$; H, n = 17 mice, time: $t_{(16)} = 6.3$, $P < .0001$; number: n = 10 mice, $t_{(9)} = 5.7$, $P = .0003$, paired *t* test). (D, I) Plots of social interaction time and number in *16p11.2del/+* mice treated with saline or MS-275 or RMD at different time points (D, time: n = 11–14 mice/group, $F_{7,161(interaction)} = 6.9$, $P < .0001$; number: n = 13–14 mice/group, $F_{7,175(interaction)} = 7.0$, $P < .0001$, 2-way repeated-measure ANOVA (rmANOVA); I, time: n = 13 mice/group, $F_{5,72} = 16.7$, $P < .0001$; number: n = 10 mice/group, $F_{5,54} = 5.8$, $P = .0002$, 1-way rmANOVA). (E, J) Bar graphs of total distance traveled (top) and time in center (bottom) in open-field locomotion tests of WT vs *16p11.2del/+* mice treated with saline or MS-275 or RMD (E, n = 16–26 mice/group, distance: $F_{1,81(treatment)} = 8.3$, $P = .0051$, $F_{1,81(genotype)} = 11.9$, $P = .0009$; time: $F_{1,81(treatment)} = 8.3$, $P = .0051$, $F_{1,81(genotype)} = 11.9$, $P = .0009$; J, n = 13-20 mice/group, distance: $F_{1,66(treatment)} = 11.9$, $P = .001$, $F_{1,66(genotype)} = 8.8$, $P = .0041$; time: $F_{1,66(treatment)} = 8.0$, $P = .0063$, $F_{1,66(genotype)} = 7.1$, $P = .0098$, 2-way ANOVA). All data are from All data are presented as mean ±SEM. In all figures, *$P < .05$, **$P < .01$, ***$P < .001$, #$P < .05$, ##$P < .01$, ###$P < .001$. *: saline vs drug, WT vs 16p^{del}, #: pre vs post.

in Figure 1A–B, the fluorescent signal of H3K9Ac in PFC neurons (NeuN-positive) was significantly lower in *16p11.2*$^{del/+}$ mice than in WT controls. Western-blot analyses (Figure 1C) also indicated a lower level of acetylated histone 3 in the PFC of *16p11.2*$^{del/+}$ mice. Treatment with the class I HDAC inhibitor romidepsin (RMD; 1 mg/kg, i.p. 3×) or MS-275 (5 mg/kg, i.p., 3×) elevated H3 acetylation close to the control level.

Class I HDAC Inhibitors Rescue Social and Cognitive Deficits of *16p11.2del/+* Mice

To verify the therapeutic effectiveness of HDAC inhibition on *16p11.2* deletion syndrome, we assessed behavioral changes in *16p11.2*$^{del/+}$ mice following the administration of class I HDAC inhibitors. We first measured their impact on social deficits in juvenile *16p11.2*$^{del/+}$ mice using the social approach test (Qin et al., 2018; Wang et al., 2018). As shown in Figure 2A–B, during the presentation of a social stimulus, *16p11.2*$^{del/+}$ mice (saline-injected) showed significantly less social interaction time and fewer social interaction numbers than WT mice (saline-injected), which was significantly elevated by MS-275 treatment (5 mg/kg, i.p., 3×). Consistent elevation of social interaction time and numbers after MS-275 treatment was found in individual *16p11.2*$^{del/+}$ mice (Figure 2C). We further examined how long the rescuing effect of MS-275 treatment can sustain by testing *16p11.2*$^{del/+}$ mice prior to and at various time points after drug treatment. As shown in Figure 2D, the significantly increased social interaction time and numbers in *16p11.2*$^{del/+}$ mice persisted for approximately 28 days post injection of MS-275, while no improvement in social preference was found with repeated measurements of saline-injected *16p11.2*$^{del/+}$ mice.

In the locomotion test, 16p11.2$^{del/+}$ mice (saline-injected) showed a significantly increased distance traveled and time in center in the open-field test compared with WT mice (saline-injected), both of which were reversed by MS-275 treatment (Figure 2E), suggesting the hyperactivity phenotype of 16p11.2 deletion mice is mitigated by HDAC inhibition. Moreover, it suggests that the altered sociability by 16p11.2 deletion or MS-275 treatment is not due to the changes in locomotion.

To verify the involvement of HDAC in the rescuing effect of MS-275 in *16p11.2*$^{del/+}$ mice, we tested another structurally different class I HDAC inhibitor, romidepsin. Romidepsin treatment (1 mg/kg, i.p., 3×) also improved the sociability of *16p11.2*$^{del/+}$ mice, as indicated by the significantly higher social interaction time and numbers in social approach tests (Figure 2F–G). The therapeutic effect of romidepsin was consistent (Figure 2H) and lasted for approximately 21 days (Figure 2I). In addition, romidepsin treatment normalized the hyperlocomotion phenotype of 16p11.2$^{del/+}$ mice (Figure 2J).

We also tested the impact of HDAC inhibitors on cognitive behaviors in *16p11.2*$^{del/+}$ mice. As shown in Figure 3A–C, in the Barnes maze (BM) test of spatial memory in which the animal was trained to use visual cues to identify an escape hole from several incorrect holes on a circular platform, *16p11.2*$^{del/+}$ mice (saline-injected) spent significantly less time around the correct hole (T1) and more time on the incorrect holes (T2); they therefore had a significantly lower spatial memory index (T1/T2) compared with WT mice (saline-injected). *16p11.2*$^{del/+}$ mice with MS-275 treatment had significantly increased T1, decreased T2, and improved spatial memory index. The rescuing effect of MS-275 was consistent (Figure 3D) and long-lasting (approximately 28 days; Figure 3E). Similar results were also obtained with romidepsin treatment (Figure 3F-J). In the novel object recognition test, compared with WT mice (saline-injected), *16p11.2*$^{del/+}$ mice (saline-injected) lost the preference for the novel object (N) over the familiar object (F). This was reversed in MS-275–treated mice, as indicated by the significantly more time on investigating N and the bigger discrimination ratio compared with saline-treated *16p11.2*$^{del/+}$ mice (Figure 3K–M). *16p11.2*$^{del/+}$ mice treated with romidepsin also had significantly improved novel object recognition memory (Figure 3N–P).

All these behavioral data suggest that a short treatment with class I HDAC inhibitors induces prolonged improvement in sociability and cognitive function as well as rescue in hyperlocomotion in the mouse model of 16p11.2 deletion syndrome.

HDAC Inhibitor Normalizes Excitability of PFC Pyramidal and Interneurons in *16p11.2del/+* Mice

To find out the physiological basis for the therapeutic effects of HDAC inhibitor on behaviors of *16p11.2*$^{del/+}$ mice, we next performed in vivo and in vitro electrophysiological recordings to examine its impact on PFC neuronal activity. First, in vivo action potential firing was compared in WT vs *16p11.2*$^{del/+}$ mice using single-unit recordings of anesthetized animals. A 16-channel probe was inserted into mPFC regions, including prelimbic and infralimbic. We recorded a total of 333 well-isolated units from WT and *16p11.2*$^{del/+}$ mice treated with saline or MS-275 (Figure 4A). Based on the trough-to-peak duration of the spike waveform (>0.25 milliseconds) and firing frequency (<10 Hz), these units are mainly from PFC pyramidal neurons (Tan et al., 2021). The mean spike rate was significantly decreased in *16p11.2*$^{del/+}$ mice compared with WT, and MS-275 treatment significantly enhanced the spike rate of mPFC units in *16p11.2*$^{del/+}$ mice (Figure 4B). These differences were also identified in the cumulative distribution plot of spike rates from the 4 groups (Figure 4C) and representative examples of recording units (Figure 4D).

To validate in vivo spike changes in *16p11.2*$^{del/+}$ mice with MS-275 treatment, we carried out in vitro whole-cell current-clamp recordings of PFC slices. In layer-V PFC pyramidal neurons from *16p11.2*$^{del/+}$ mice, the spikes elicited by various depolarizing currents were significantly reduced, which were elevated to the control level by MS-275 treatment (Figure 5A). Moreover, the diminished frequency of synaptic-driven spontaneous action potentials in *16p11.2*$^{del/+}$ PFC pyramidal neurons was also restored in MS-275-treated *16p11.2*$^{del/+}$ mice (Figure 5B). Because E/I balance disruption is a well-known hypothesis in autism (Sohal and Rubenstein, 2019), we next recorded the neuronal activities in layer I-II PFC fast-spiking (FS) interneurons, which were identified from their morphology and firing pattern. We found a significant increase of the frequencies of evoked action potentials and spontaneous action potentials in *16p11.2*$^{del/+}$ mice, which was brought down to the control level by MS-275 treatment (Figure 5C–D). Taken together, these data indicate that *16p11.2*$^{del/+}$ mice have hypoactive PFC pyramidal neurons and hyperactive PFC interneurons, and the disrupted E/I balance is restored by HDAC inhibition.

HDAC Inhibitor Normalizes NMDAR- and $GABA_AR$-Mediated Synaptic Responses in PFC Pyramidal Neurons of *16p11.2del/+* Mice

To understand the synaptic mechanism that may underlie the effects of MS-275 on PFC neuronal activity, we examined glutamatergic excitation and GABAergic inhibition in PFC pyramidal neurons of *16p11.2*$^{del/+}$ mice. Our previous study found that NMDAR-mediated excitatory postsynaptic currents

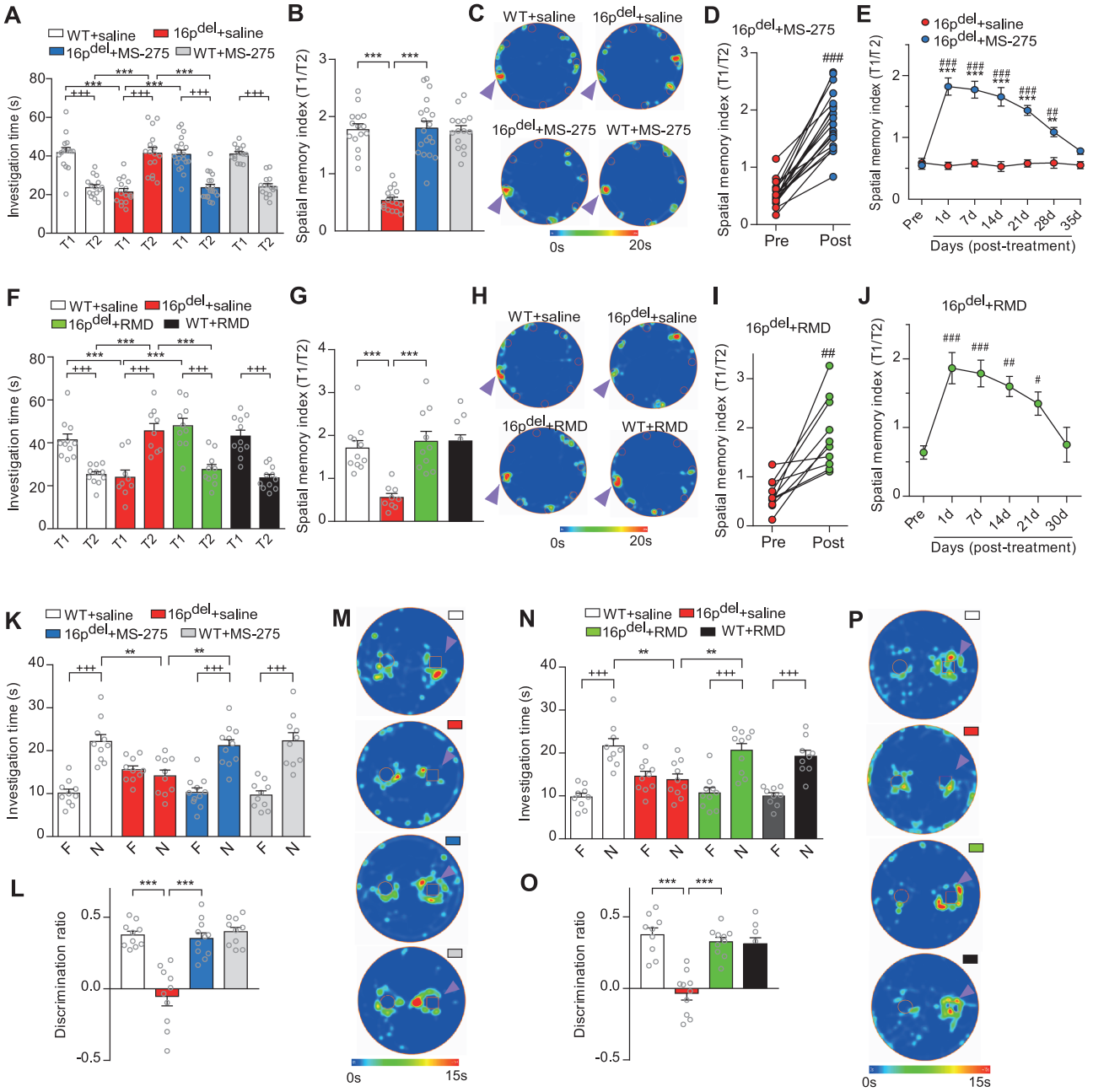

Figure 3. Treatment with HDAC inhibitors induces sustained amelioration of cognitive deficits in *16p11.2del/+* mice. (A, F) Bar graphs of the time spent on investigating correct (T1) and incorrect (T2) holes in Barnes maze (BM) tests of WT vs *16p11.2del/+* mice treated with saline or MS-275 (5 mg/kg, i.p., 3×) or romidepsin (RMD) (1 mg/kg, i.p. 3×) (A, n = 15–19 mice/group, $F_{3,122(interaction)} = 52.3$, $P < .0001$; F, n = 9–11 mice/group, $F_{3,74(interaction)} = 26.7$, $P < .0001$, 2-way ANOVA). (B, G) Bar graphs of spatial memory index (T1/T2) in BM tests of the 4 groups (B, n = 15–19 mice/group, $F_{1,61(interaction)} = 48.8$, $P < .0001$; F, n = 9–11 mice/group, $F_{1,37(interaction)} = 11.5$, $P < .0001$, 2-way ANOVA). (C, H) Representative heatmaps showing the time spent on investigating correct and incorrect holes in BM tests of different groups. The arrow points to the correct hole. (D, I) Scatter plots of spatial memory index of individual *16p11.2del/+* mice before and after MS-275 or RMD treatment (D, n = 19 mice, $t_{(18)} = 12.2$, $P < .0001$; I, n = 10 mice, $t_{(9)} = 4.7$, $P = .0011$, paired *t* test). (E, J) Plots of spatial memory index in*16p11.2del/+* mice treated with saline or MS-275 or RMD at different time points (E, n = 12–15 mice/group, $F_{6,150(interaction)} = 16.7$, $P < .0001$, 2-way repeated-measure ANOVA (rmANOVA); J, n = 10 mice/group, $F_{5,54} = 7.7$, $P = .0011$, 1-way rmANOVA). (K, N) Bar graphs of the time spent on investigating familiar (F) and novel (N) objects in Novel Object Recognition (NOR) tests of WT vs *16p11.2del/+* mice treated with saline or MS-275 or RMD (K, n = 10–11 mice/group, $F_{3,74(interaction)} = 12.8$, $P < .0001$; N, n = 9–10 mice/group, $F_{3,68(interaction)} = 9.9$, $P < .0001$, 2-way ANOVA). (L, O) Bar graphs of discrimination ratio in NOR tests of the 4 groups (L, n = 10–11 mice/group, $F_{1,37(interaction)} = 21.0$, $P < .0001$; *n* = 9–10 mice/group, $F_{1,34(interaction)} = 25.1$, $P < .0001$, 2-way ANOVA). (M, P) Representative heatmaps showing the time spent on investigating familiar and novel objects in NOR tests of different groups. The arrow points to the novel object. All data are presented as mean ±SEM. In all figures, *$P < .05$, **$P < .01$, ***$P < .001$; #$P < .05$, ##$P < .01$, ###$P < .001$; ++$P < .01$, +++$P < .001$. *: saline vs drug, WT vs 16p^{del}, #: pre vs post, +: T1 vs T2 or F vs N.

(NMDAR-EPSC) significantly diminished in PFC pyramidal neurons from *16p11.2*$^{del/+}$ mice, while AMPAR-mediated excitatory postsynaptic currents were largely unchanged (Wang et al., 2018), so we focused on NMDAR-EPSC recordings in this study. As shown in Figure 6A, saline-injected *16p11.2*$^{del/+}$ mice did have significantly reduced NMDAR-EPSC in PFC pyramidal neurons compared with WT mice, while MS-275 treatment elevated it to the control level. PPR, a readout of presynaptic transmitter

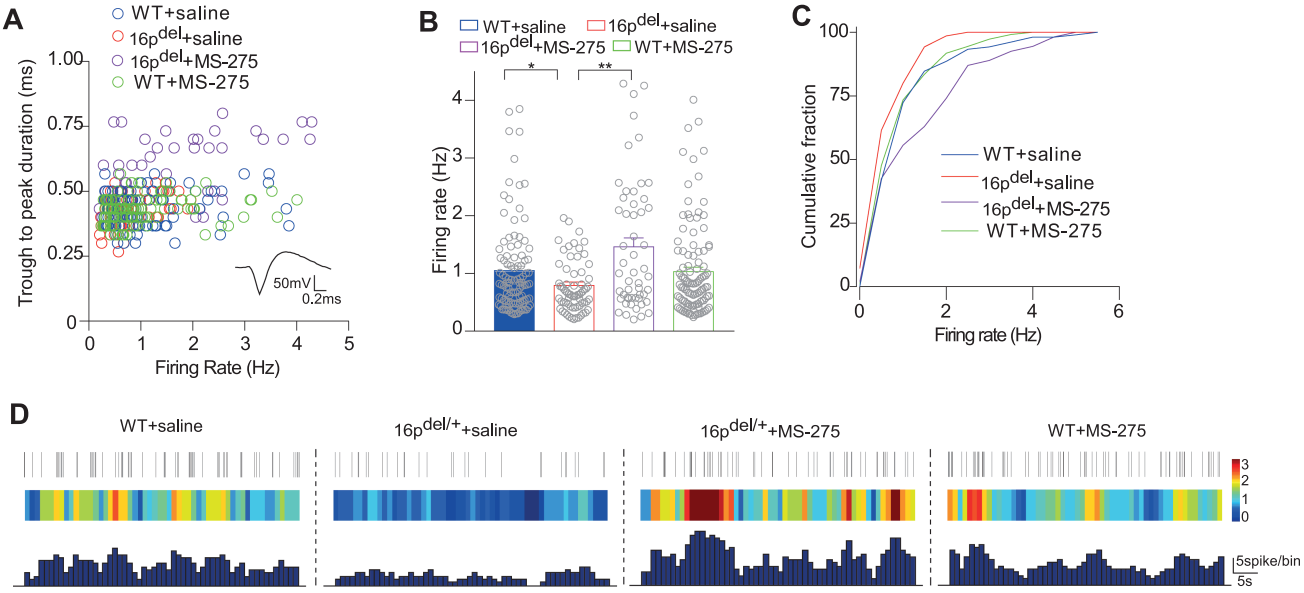

Figure 4. HDAC inhibitor restores the diminished in vivo spike activity in PFC of *16p11.2del/+* mice. (A) Scatter plots of firing rate and through-to-peak duration of recorded mPFC units in WT (n = 103 units/8 mice), *16p11.2del/+* (n = 68 units/6 mice), *16p11.2del/+* +MS-275 (n = 53 units/6 mice) and WT+MS-275 (n = 109 units/8 mice) group. (B) Bar graphs of firing rate of recorded units in the 4 groups ($F_{1,329(interaction)} = 15.6$, $P < .0001$, 2-way ANOVA). (C) Cumulative frequency distribution plots of recorded units. (D) Representative in vivo recording data from the 4 groups. Top: raster plots; Middle: heat maps; Bottom: histogram of spikes of a recorded unit. All data are presented as mean ±SEM. In all figures, $^{*}P < .05$, $^{**}P < .01$.

release, of NMDAR-EPSC was unchanged in any of these groups (Figure 6B).

Disturbed synaptic balance in the cerebral cortex has been reported in different animal models of ASD (Antoine et al., 2019; Qin et al., 2021b), and the GABAergic synaptic transmission in PFC pyramidal neurons in 16p11.2 deletion mice has not been reported. Next, we compared GABAergic synaptic transmission in PFC pyramidal neurons in WT and *16p11.2*$^{del/+}$ mice. Whole-cell voltage-clamp recordings revealed a significant increase of $GABA_A$R-mediated inhibitory postsynaptic currents ($GABA_A$R-IPSC) evoked by synaptic stimulations of various intensities in layer V PFC pyramidal neurons from *16p11.2*$^{del/+}$ mice, and MS-275 treatment brought them down to similar levels to WT mice (Figure 7A). PPR of $GABA_A$R-IPSC was also significantly decreased (double pulse interval at 30 milliseconds) in *16p11.2*$^{del/+}$ mice, which was elevated by MS-275 treatment (Figure 7B). Furthermore, MS-275 treatment normalized the significantly increased frequency of spontaneous IPSC and miniature IPSC in *16p11.2*$^{del/+}$ mice (Figure 7C–E). These data suggest that MS-275-induced dampening of the elevated GABA signaling in *16p11.2*$^{del/+}$ mice may result from normalizing the increased presynaptic GABA release in agreement with MS-275–induced normalization of the increased firing of PFC fast-spiking interneurons in *16p11.2*$^{del/+}$ mice.

To further investigate the molecular mechanisms that may contribute to the altered GABAergic transmission in *16p11.2*$^{del/+}$ mice, we examined the mRNA level of several genes related to GABA transporters, receptors, or GABAergic interneurons. As shown in Figure 7F, the qRT-PCR profiling revealed a significant decrease (close to 50%) of *Mapk3*, one of the genes within *16p11.2* genetic locus, in PFC of *16p11.2*$^{del/+}$ mice, consistent with the copy number deletion of this chromosomal region in these mice. The mRNA levels of *Slc6a1* (encoding GABA transporter GAT-1) and *Pvalb* (encoding parvalbumin) were significantly increased in the PFC of *16p11.2*$^{del/+}$ mice, which may underlie the elevated GABAergic signaling. Moreover, the neuronal activity marker, *Arc*, was significantly reduced in PFC of *16p11.2*$^{del/+}$ mice, consistent with the reduced PFC pyramidal neuronal activity found in both in vivo and in vitro recordings.

Taken together, these data indicate that *16p11.2*$^{del/+}$ mice have NMDAR hypofunction and GABA hyperfunction in PFC pyramidal neurons, and the disrupted synaptic balance is restored by HDAC inhibition.

Discussion

Aberrations in chromatin remodeling and synaptic homeostasis have been strongly implicated in autism by genetic screenings (De Rubeis et al., 2014; Satterstrom et al., 2020). Here we provide—for the first time, to our knowledge—electrophysiological and behavioral evidence demonstrating that inhibiting class I HDACs restores synaptic functions in the PFC of *16p11.2*$^{del/+}$ mice, leading to the long-lasting rescue of social and cognitive deficits as well as the normalization of hyperlocomotion. In ASD models with the haploinsufficiency of *Shank3* gene, which encodes a master scaffolding protein in the postsynaptic density of glutamatergic synapses (Naisbitt et al., 1999) and is causally linked to 22q13.3 deletion syndrome (Betancur and Buxbaum, 2013; Guilmatre et al., 2014), class I HDAC inhibitors like romidepsin and MS-275 also show strong therapeutic potentials (Ma et al., 2018; Qin et al., 2018; Zhang et al., 2021). These preclinical studies have demonstrated that targeting epigenetic enzymes is a promising avenue for autism treatment.

Microdeletion of the 16p11.2 region is associated with several syndromes largely characterized by social, cognitive, and intellectual deficits (Portmann et al., 2014; Tian et al., 2015; Yang et al., 2015a, 2015b; Arbogast et al., 2016). Consistently, we have found that *16p11.2*$^{del/+}$ mice exhibit significantly reduced social interactions in social approach tests, spatial memory and recognition memory deficits, as well as hyperactivities in open field. These behavioral abnormalities are ameliorated by a short

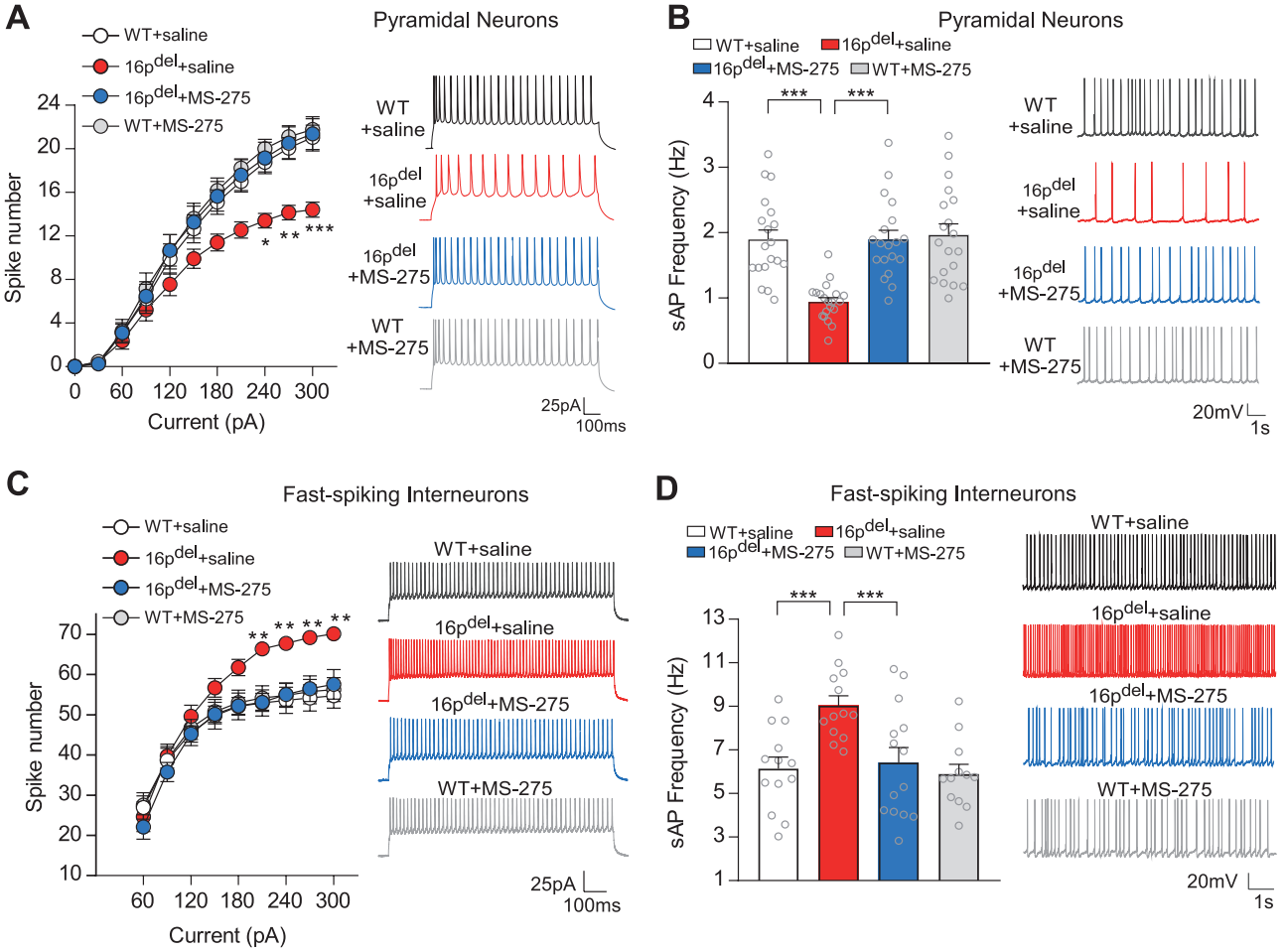

Figure 5. HDAC inhibitor normalizes the excitability of PFC pyramidal neurons and fast-spiking (FS) interneurons in *16p11.2del/+* mice. (A, C) Plot of the number of action potential spikes evoked by different depolarizing currents in PFC pyramidal neurons or FS interneurons from WT and *16p11.2del/+* mice treated with saline or MS-275 (A, n = 17–20 cells/4 mice/group, $F_{30,700(interaction)} = 3.6$, $P < .0001$; C, n = 9–12 cells/3–5 mice/group, $F_{24,328(interaction)} = 7.3$, $P < .0001$, 2-way rmANOVA). Inset: representative evoked action potential traces. (B, D) Bar graphs showing the frequency of synaptic-driven spontaneous AP in PFC pyramidal neurons or FS interneurons from the 4 groups (B, n = 19–20 cells/4 mice each group, $F_{1,73(interaction)} = 11.1$, $P = .0013$; D, n = 12-14 cells/4 mice/group, $F_{1,48(interaction)} = 4.6$, $P = .038$, 2-way ANOVA). Inset: representative sAP traces. All data are presented as mean ±SEM. In all figures, $^{*}P < .05$, $^{**}P < .01$, $^{***}P < .001$.

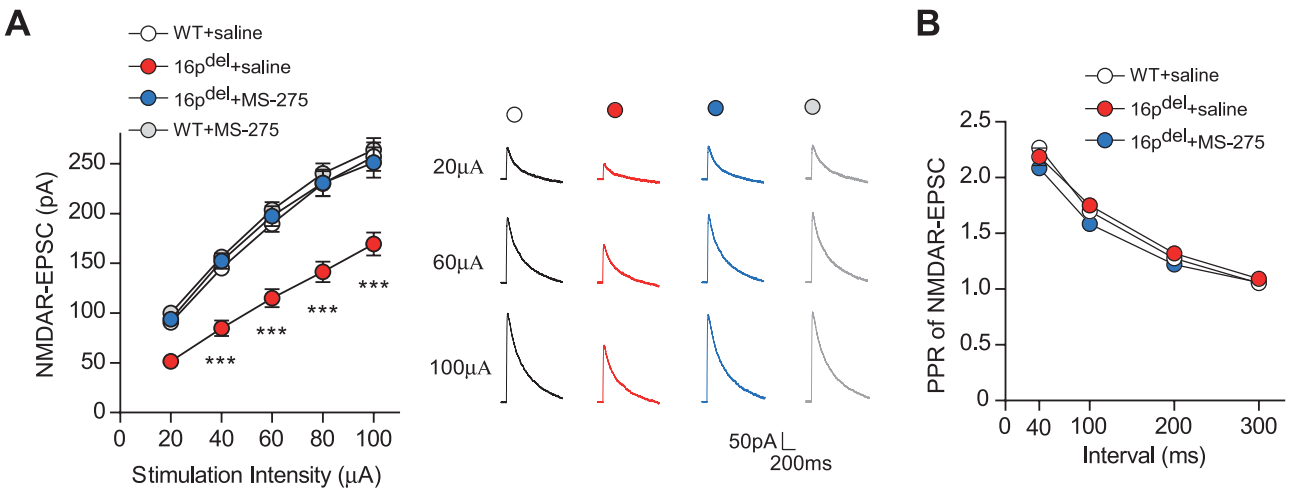

Figure 6. HDAC inhibitor restores NMDAR-mediated synaptic response in PFC pyramidal neurons of *16p11.2del/+* mice. (A) Input/output curves of NMDAR-EPSC in PFC pyramidal neurons from WT and *16p11.2del/+* mice treated with saline or MS-275 (n = 24–27 cells/5 mice/group, $F_{3,100(group)} = 18.4$, $P < .0001$, 2-way repeated-measure ANOVA [rmANOVA]). Inset: representative NMDAR-EPSC traces. (B) Plot of paired-pulse ratio (PPR) of NMDAR-EPSC evoked by double pulses with various intervals in PFC pyramidal neurons from the 4 groups (n = 13–17 cells/4 mice/group, $F_{2,41(group)} = 2.7$, $P = .08$, 2-way rmANOVA). All data are presented as mean ±SEM. In all figures, $^{***}P < .001$.

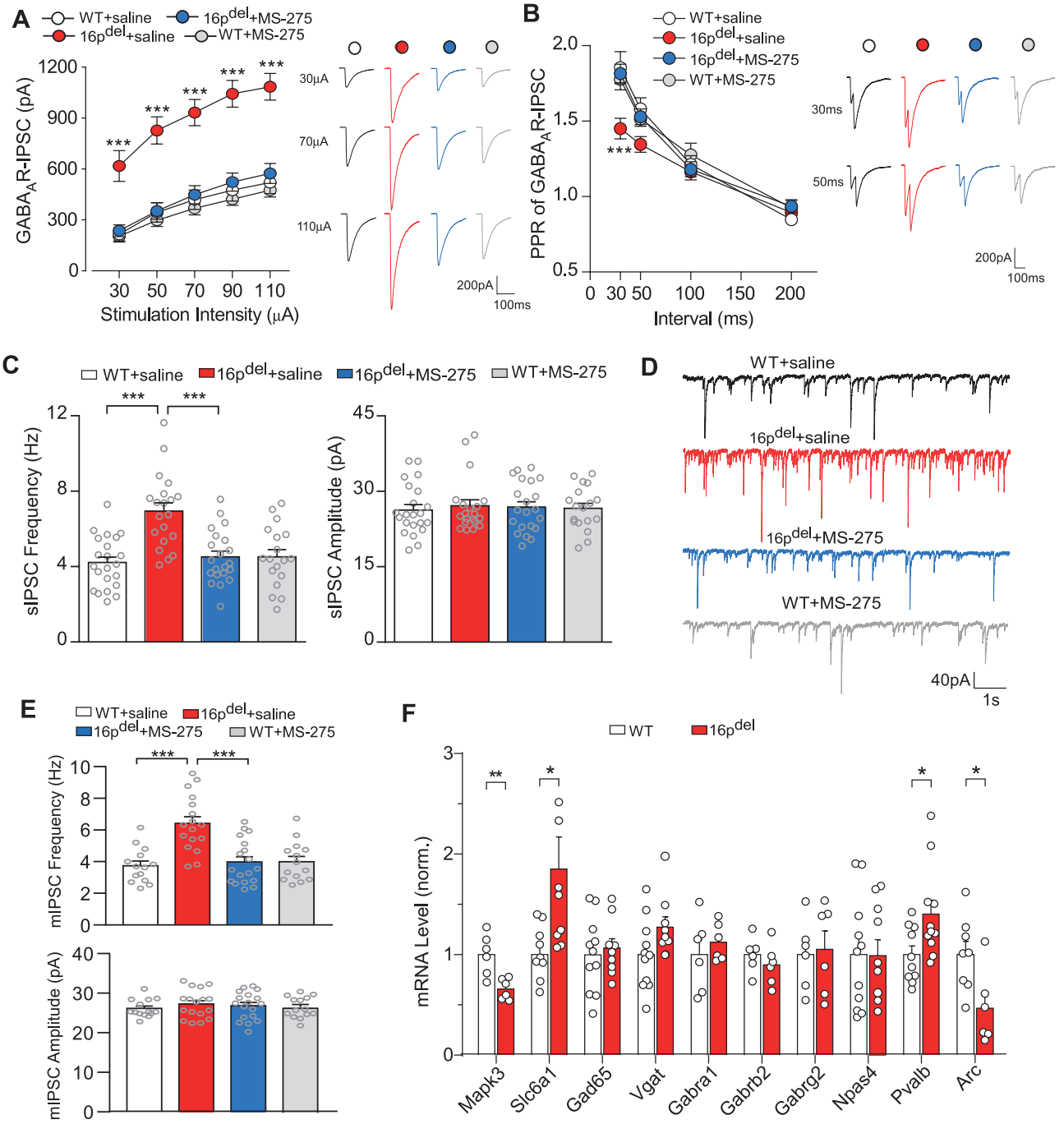

Figure 7. HDAC inhibitor normalizes GABAergic transmission in PFC pyramidal neurons of *16p11.2del/+* mice. (A) Input/output curves of GABA$_A$R-IPSC in PFC pyramidal neurons from WT and *16p11.2del/+* mice treated with saline or MS-275 (n = 17-23 cells/5–6 mice/group, $F_{3,78(group)} = 20.5$, $P < .0001$, 2-way repeated-measure ANOVA [rmANOVA]). Inset: representative GABA$_A$R-IPSC traces. (B) Plot of PPR of GABA$_A$R-IPSC evoked by double pulses with various intervals in PFC pyramidal neurons from the 4 groups (n = 15–17 cells/5–6 mice/group, $F_{3,59(group)} = 4.5$, $P = .0065$, 2-way rmANOVA). Inset: representative traces. (C, E) Bar graphs of spontaneous and miniature IPSC in PFC pyramidal neurons from the 4 groups. (C, n = 18–22 cells/5–6 mice/group, Frequency: $F_{1,77(interaction)} = 14.8$, $P = .0003$, Amplitude: $F_{1,77(interaction)} = 0.07$, $P = .8$; E, n = 14–18 cells/3 mice/group, Frequency: $F_{1,59(interaction)} = 13.4$, $P = .0004$, Amplitude: $F_{1,59(interaction)} = 0.2$, $P = .6$, 2-way ANOVA). (D) Representative spontaneous IPSC traces. (F) Bar graph of mRNA levels of GABA-related genes in PFC of WT vs *16p11.2del/+* mice (Mapk3: n = 6 mice/group, $t_{(10)} = 3.7$, $P = .0044$, Slc6a1: n = 9–10 mice/group, $t_{(17)} = 2.7$, $P = .015$, Pvalb, n = 10–11 mice/group, $t_{(19)} = 2.4$, $P = .025$, Arc: n = 6–8 mice/group, $t_{(12)} = 2.7$, $P = .019$, unpaired *t* test). All data are presented as mean ±SEM. In all figures, $^*P < .05$, $^{**}P < .01$, $^{***}P < .001$.

(3 days) treatment with MS-275 or romidepsin. More importantly, the rescuing effects sustain for a long time (3–4 weeks), outlasting the presence of these compounds. This suggests that targeting epigenetic enzymes may trigger gene expression changes that could lead to prolonged alterations of downstream biological processes.

The earlier studies of 16p11.2 deletion mice (Horev et al., 2011; Portmann et al., 2014) did not demonstrate sex-specific behavioral changes. However, female-specific stress-induced anxiety (Giovanniello et al., 2021), male-specific deficits in sleep (Angelakos et al., 2017; Lu et al., 2019) and natural reward learning (Grissom et al., 2018), and sex-specific basic metabolism

(Menzies et al., 2021) have been reported in 16p11.2 deletion mice. Our behavioral tests of social approach, locomotion, and cognitive behaviors did not find significant sex differences. It awaits to be tested whether HDAC inhibition rescues the sex-specific phenotypes in 16p11.2 deletion mice.

To find out the physiological basis of these behavioral changes, we examined neuronal excitability and synaptic function in *16p11*$^{del/+}$ mice. We have for the first time, to our knowledge, found elevated excitability (hyperactivity) of PFC fast-spiking interneurons (GABAergic) and decreased in vivo spike activity in PFC pyramidal neurons (glutamatergic) of *16p11*$^{del/+}$ mice, which is accompanied by the diminished excitability (hypoactivity) of PFC pyramidal neurons in vitro and prominent NMDAR hypofunction in *16p11*$^{del/+}$ mice, consistent with our previous findings (Wang et al., 2018). In addition, we found for the first time, to our knowledge, that PFC pyramidal neurons of *16p11*$^{del/+}$ mice exhibit significantly augmented inhibitory synaptic responses, which is likely due to the presynaptic change in GABA release. Remarkably, MS-275 treatment reverses the E/I imbalance and synaptic alterations in the PFC of *16p11*$^{del/+}$ mice. Prior studies with a wide variety of ASD models have shown that the manifestation of autistic phenotypes could be attributed to the disrupted E/I balance (Lee et al., 2017; Antoine et al., 2019; Qin et al., 2021b), glutamatergic function (Duffney et al., 2013; Qin et al., 2018; Wang et al., 2018; Rapanelli et al., 2021), or GABA system (Jung et al., 2017; Lee et al., 2021; Rein et al., 2021). The restoration of PFC synaptic physiology by a class I HDAC inhibitor provides a mechanistic basis for its effectiveness in treating behavioral symptoms of *16p11*$^{del/+}$ mice.

While we focused the measurement of cellular changes in PFC because of the key role of this brain region in regulating social and cognitive behaviors measured here (Duffney et al., 2015; Qin et al., 2018; Zheng et al., 2019; Cao et al., 2020; Rapanelli et al., 2021; Wang et al., 2021), the data from systemic administrations of HDAC inhibitors are still not adequate to draw a causal link between cellular changes in PFC and behavioral changes in16p11$^{del/+}$ mice. Future studies will examine whether there are cellular changes in other brain regions and what is responsible for the restoration of behavioral phenotypes.

One challenge is to find molecular targets downstream of HDAC inhibition involved in the amelioration of synaptic deficits. qPCR profiling has revealed the significantly increased GABA system genes (e.g., *Slc6a1* and *Pvalb*) and the significantly decreased synaptic plasticity gene *Arc* in PFC of *16p11.2*$^{del/+}$ mice, providing new evidence that they could be direct targets of MS-275 treatment involved in synaptic recovery. Our previous transcriptomic studies have found that the majority (approximately 88%) of the >200 downregulated genes in *Shank3*-deficient mice are restored by romidepsin treatment, and these genes are highly enriched in actin cytoskeleton-mediated transport, signal transduction pathways, and developmental processes (Qin et al., 2018). Future studies will identify gene targets of HDAC inhibition that play a causal role in the synaptic and behavioral rescue of *16p11.2*$^{del/+}$ mice.

Acknowledgments

We thank Xiaoqing Chen, Tiaotiao Liu, Luye Qin, Jamal B. Williams, and Kaijie Ma for their excellent technical support. This work was supported by grants from the Nancy Lurie Marks Family Foundation and National Institutes of Health (MH112237) to Z.Y.

Author Contributions

W.W. designed experiments, performed behavioral, and electrophysiological experiments, analyzed data, and wrote parts of the draft. T.T. performed in vivo recording experiments and data analyses. Q.C. performed immunohistochemical experiments and analyzed data. F.Z. performed western blot, parts of behavioral experiments, and analyzed data. B.R. performed qPCR and analyzed data. W.D. performed parts of behavioral experiments and analyzed data. Z.Y. designed experiments, supervised the project, and wrote the paper.

Interests Statement

The authors have no financial or other interests in this study.

References

Angelakos CC, Watson AJ, O'Brien WT, Krainock KS, Nickl-Jockschat T, Abel T (2017) Hyperactivity and male-specific sleep deficits in the 16p11.2 deletion mouse model of autism. Autism Res 10:572–584.

Antoine MW, Langberg T, Schnepel P, Feldman DE (2019) Increased excitation-inhibition ratio stabilizes synapse and circuit excitability in four autism mouse models. Neuron 101:648–661.e4.e644.

Arbogast T, Ouagazzal A-M, Chevalier C, Kopanitsa M, Afinowi N, Migliavacca E, Cowling BS, Birling M-C, Champy M-F, Reymond A, Herault Y (2016) Reciprocal effects on neurocognitive and metabolic phenotypes in mouse models of 16p11.2 deletion and duplication syndromes. PLoS Genet 12:e1007095.

Betancur C, Buxbaum JD (2013) SHANK3 haploinsufficiency: a "common" but underdiagnosed highly penetrant monogenic cause of autism spectrum disorders. Mol Autism 4:17.

Blumenthal I, Ragavendran A, Erdin S, Klei L, Sugathan A, Guide JR, Manavalan P, Zhou JQ, Wheeler VC, Levin JZ, Ernst C, Roeder K, Devlin B, Gusella JF, Talkowski ME (2014) Transcriptional consequences of 16p11.2 deletion and duplication in mouse cortex and multiplex autism families. Am J Hum Genet 94:870–883.

Cao Q, Wang W, Williams JB, Yang F, Wang ZJ, Yan Z (2020) Targeting histone K4 trimethylation for treatment of cognitive and synaptic deficits in mouse models of Alzheimer's disease. Sci Adv 6:eabc8096.

Contestabile A, Sintoni S (2013) Histone acetylation in neurodevelopment. Curr Pharm Des 19:5043–5050.

De Rubeis S, et al. (2014) Synaptic, transcriptional and chromatin genes disrupted in autism. Nature 515:209–215.

Duffney LJ, Wei J, Cheng J, Liu W, Smith KR, Kittler JT, Yan Z (2013) Shank3 deficiency induces NMDA receptor hypofunction via an actin-dependent mechanism. J Neurosci 33:15767–15778.

Duffney LJ, Zhong P, Wei J, Matas E, Cheng J, Qin L, Ma K, Dietz DM, Kajiwara Y, Buxbaum JD, Yan Z (2015) Autism-like deficits in shank3-deficient mice are rescued by targeting actin regulators. Cell Rep 11:1400–1413.

Fernandez BA, Roberts W, Chung B, Weksberg R, Meyn S, Szatmari P, Joseph-George AM, Mackay S, Whitten K, Noble B, Vardy C, Crosbie V, Luscombe S, Tucker E, Turner L, Marshall CR, Scherer SW (2010) Phenotypic spectrum associated with de novo and inherited deletions and duplications at 16p11.2 in individuals ascertained for diagnosis of autism spectrum disorder. J Med Genet 47:195–203.

Giovanniello J, Ahrens S, Yu K, Li B (2021) Sex-specific stress-related behavioral phenotypes and central amygdala dysfunction in

a mouse model of 16p11.2 microdeletion. Biol. Psychiatry 1:59–69.

Grissom NM, McKee SE, Schoch H, Bowman N, Havekes R, O'Brien WT, Mahrt E, Siegel S, Commons K, Portfors C, Nickl-Jockschat T, Reyes TM, Abel T (2018) Male-specific deficits in natural reward learning in a mouse model of neurodevelopmental disorders. Mol Psychiatry 23:544–555.

Guilmatre A, Huguet G, Delorme R, Bourgeron T (2014) The emerging role of SHANK genes in neuropsychiatric disorders. Dev Neurobiol 74:113–122.

Hanson E, Nasir RH, Fong A, Lian A, Hundley R, Shen Y, Wu BL, Holm IA, Miller DT; 16p11.2 Study Group Clinicians (2010) Cognitive and behavioral characterization of 16p11.2 deletion syndrome. J Dev Behav Pediatr 31:649–657.

Horev G, Ellegood J, Lerch JP, Son YE, Muthuswamy L, Vogel H, Krieger AM, Buja A, Henkelman RM, Wigler M, Mills AA (2011) Dosage-dependent phenotypes in models of 16p11.2 lesions found in autism. Proc Natl Acad Sci USA 108:17076–17081.

Jung EM, Moffat JJ, Liu J, Dravid SM, Gurumurthy CB, Kim WY (2017) Arid1b haploinsufficiency disrupts cortical interneuron development and mouse behavior. Nat Neurosci 20:1694–1707.

Kumar RA, KaraMohamed S, Sudi J, Conrad DF, Brune C, Badner JA, Gilliam TC, Nowak NJ, Cook EH Jr, Dobyns WB, Christian SL (2008) Recurrent 16p11.2 microdeletions in autism. Hum Mol Genet 17:628–638.

Lee E, Lee J, Kim E (2017) Excitation/inhibition imbalance in animal models of autism spectrum disorders. Biol Psychiatry 81:838–847.

Lee E, et al. (2021) Excitatory synapses and gap junctions cooperate to improve Pv neuronal burst firing and cortical social cognition in Shank2-mutant mice. Nat Commun 12:5116.

Lu HC, Pollack H, Lefante JJ, Mills AA, Tian D (2019) Altered sleep architecture, rapid eye movement sleep, and neural oscillation in a mouse model of human chromosome 16p11.2 microdeletion. Sleep 42:zsy253.

Ma K, Qin L, Matas E, Duffney LJ, Liu A, Yan Z (2018) Histone deacetylase inhibitor MS-275 restores social and synaptic function in a Shank3-deficient mouse model of autism. Neuropsychopharmacology 43:1779–1788.

Menzies C, Naz S, Patten D, Alquier T, Bennett BM, Lacoste B (2021) Distinct basal metabolism in three mouse models of neurodevelopmental disorders. eNeuro 8:ENEURO.0292-20.2021.

Naisbitt S, Kim E, Tu JC, Xiao B, Sala C, Valtschanoff J, Weinberg RJ, Worley PF, Sheng M (1999) Shank, a novel family of postsynaptic density proteins that binds to the NMDA receptor/PSD-95/GKAP complex and cortactin. Neuron 23:569–582.

Ouellette J, et al. (2020) Vascular contributions to 16p11.2 deletion autism syndrome modeled in mice. Nat Neurosci 23:1090–1101.

Portmann T, Yang M, Mao R, Panagiotakos G, Ellegood J, Dolen G, Bader PL, Grueter BA, Goold C, Fisher E (2014) Behavioral abnormalities and circuit defects in the basal ganglia of a mouse model of 16p11.2 deletion syndrome. Cell Reports 7:1077–1092.

Qin L, Ma K, Wang ZJ, Hu Z, Matas E, Wei J, Yan Z (2018) Social deficits in Shank3-deficient mouse models of autism are rescued by histone deacetylase (HDAC) inhibition. Nat Neurosci 21:564–575.

Qin L, Ma K, Yan Z (2021a) Rescue of histone hypoacetylation and social deficits by ketogenic diet in a Shank3 mouse model of autism. Neuropsychopharmacology 47:1271–1279.

Qin L, Williams JB, Tan T, Liu T, Cao Q, Ma K, Yan Z (2021b) Deficiency of autism risk factor ASH1L in prefrontal cortex induces epigenetic aberrations and seizures. Nat Commun 12:6589.

Rapanelli M, Tan T, Wang W, Wang X, Wang ZJ, Zhong P, Frick L, Qin L, Ma K, Qu J, Yan Z (2021) Behavioral, circuitry, and molecular aberrations by region-specific deficiency of the high-risk autism gene Cul3. Mol Psychiatry 26:1491–1504.

Rein B, Tan T, Yang F, Wang W, Williams J, Zhang F, Mills A, Yan Z (2021) Reversal of synaptic and behavioral deficits in a 16p11.2 duplication mouse model via restoration of the GABA synapse regulator Npas4. Mol Psychiatry 26:1967–1979.

Rein B, Yan Z (2020) 16p11.2 Copy number variations and neurodevelopmental disorders. Trends Neurosci. 43:886–901.

Rosenfeld JA, Coppinger J, Bejjani BA, Girirajan S, Eichler EE, Shaffer LG, Ballif BC (2010) Speech delays and behavioral problems are the predominant features in individuals with developmental delays and 16p11.2 microdeletions and microduplications. J Neurodev Disord 2:26–38.

Satterstrom FK, et al. (2020) Large-scale exome sequencing study implicates both developmental and functional changes in the neurobiology of autism. Cell 180:568–584.e23.e523.

Shinawi M, et al. (2010) Recurrent reciprocal 16p11.2 rearrangements associated with global developmental delay, behavioural problems, dysmorphism, epilepsy, and abnormal head size. J Med Genet 47:332–341.

Sohal VS, Rubenstein JLR (2019) Excitation-inhibition balance as a framework for investigating mechanisms in neuropsychiatric disorders. Mol Psychiatry 24:1248–1257.

Tan T, Wang W, Liu T, Zhong P, Conrow-Graham M, Tian X, Yan Z (2021) Neural circuits and activity dynamics underlying sex-specific effects of chronic social isolation stress. Cell Rep 34:108874.

Tian D, Stoppel LJ, Heynen AJ, Lindemann L, Jaeschke G, Mills AA, Bear MF (2015) Contribution of mGluR5 to hippocampal pathophysiology in a mouse model of human chromosome 16p11.2 microdeletion. Nat Neurosci 18:182–184.

Tsankova N, Renthal W, Kumar A, Nestler EJ (2007) Epigenetic regulation in psychiatric disorders. Nat Rev Neurosci 8:355–367.

Walsh JJ, Christoffel DJ, Heifets BD, Ben-Dor GA, Selimbeyoglu A, Hung LW, Deisseroth K, Malenka RC (2018) 5-HT release in nucleus accumbens rescues social deficits in mouse autism model. Nature 560:589–594.

Wang W, Rein B, Zhang F, Tan T, Zhong P, Qin L, Yan Z (2018) Chemogenetic activation of prefrontal cortex rescues synaptic and behavioral deficits in a mouse model of 16p11.2 deletion syndrome. J Neurosci 38:5939–5948.

Wang W, Cao Q, Tan T, Yang F, Williams JB, Yan Z (2021) Epigenetic treatment of behavioral and physiological deficits in a tauopathy mouse model. Aging Cell 20:e13456.

Weiss LA, et al. (2008) Association between microdeletion and microduplication at 16p11.2 and autism. N Engl J Med 358:667–675.

Yan Z, Rein B (2022) Mechanisms of synaptic transmission dysregulation in the prefrontal cortex: pathophysiological implications. Mol Psychiatry 27:445–465.

Yang M, Lewis FC, Sarvi MS, Foley G, Crawley JN (2015a) 16p11.2 deletion mice display cognitive deficits in touchscreen learning and novelty recognition tasks. Learn Mem 22:622–632.

Yang M, Mahrt EJ, Lewis F, Foley G, Portmann T, Dolmetsch RE, Portfors CV, Crawley JN (2015b) 16p11.2 deletion syndrome

mice display sensory and ultrasonic vocalization deficits during social interactions. Autism Res 8:507–521.

Yin X, Jones N, Yang J, Asraoui N, Mathieu ME, Cai L, Chen SX (2021) Delayed motor learning in a 16p11.2 deletion mouse model of autism is rescued by locus coeruleus activation. Nat Neurosci 24:646–657.

Zhang F, Rein B, Zhong P, Shwani T, Conrow-Graham M, Wang ZJ, Yan Z (2021) Synergistic inhibition of histone modifiers produces therapeutic effects in adult Shank3-deficient mice. Transl Psychiatry 11:99.

Zheng Y, Liu A, Wang ZJ, Cao Q, Wang W, Lin L, Ma K, Zhang F, Wei J, Matas E, Cheng J, Chen GJ, Wang X, Yan Z (2019) Inhibition of EHMT1/2 rescues synaptic and cognitive functions for Alzheimer's disease. Brain 142:787–807.

Zhong P, Yan Z (2016) Distinct physiological effects of dopamine D4 receptors on prefrontal cortical pyramidal neurons and fast-spiking interneurons. Cereb Cortex 26:180–191.

Zufferey F, et al. (2012) A 600 kb deletion syndrome at 16p11.2 leads to energy imbalance and neuropsychiatric disorders. J Med Genet 49:660–668.